Water structures on Pb(100) and (111) surface studied with the Interface force field

Oskar Cheong[a,b,c], Michael Eikerling[a,b,c], Piotr M. Kowalski[a,c,*]

[a] *Institute of Energy and Climate Research (IEK-13), Forschungszentrum Jülich, Wilhelm-Johnen-Straße, 52425 Jülich, Germany*
[b] *Chair of Theory and Computation of Energy Materials, Faculty of Georesources and Materials Enginering, RWTH Aachen University, Intzestrasse 5, 52072 Aachen, Germany*
[c] *JARA Energy & Center for Simulation and Data Science (CSD), 52425 Jülich, Germany*

Abstract

We performed classical molecular dynamics (CMD) simulations of water structures on Pb(100) and (111) surfaces. The main objective was to test the capability of interface force field to reproduce water structures obtained from more computationally intensive *ab initio* molecular dynamics (AIMD) simulations. At the same length and time scales we find good agreement between water structures obtained with both approaches. However, much longer trajectories (ns vs. ps scale) that can be simulated with CMD led to the formation of different, more stable water structures, which were validated by supplementary *ab initio* calculations. CMD simulations performed for interface models with larger surface size revealed significant surface cell size effects, implying that the small simulation cells permitted by AIMD could be insufficient to obtain properly equilibrated water structures. These results indicate the usefulness and advantage of CMD simulations that employ the interface force field for the rapid sampling of more realistic time and length scales in simulations of metal-aqueous solution interfaces.

Keywords:

ab initio calculations, water structures, metal-water interface, classical molecular dynamics simulations, interface force field

*Corresponding author: Piotr M. Kowalski Tel.: +49 2461 61 85928, E-mail: p.kowalski@fz-juelich.de

1. Introduction

Interactions between solvents and metal surfaces play a significant role in interfacial electrochemical processes [1]. They strongly affect the activity and selectivity of surface electrochemical processes, including oxygen and hydrogen evolution or CO_2 reduction reactions [2, 3, 4, 5]. While significant efforts have focused on understanding the formation of water structures on metal surfaces, both computationally [6, 7, 8, 9] and experimentally [10, 11, 12], no conclusive model has emerged. For instance, Doering and Madey [13] experimentally showed the existence of an ice-like water bilayer on the close-packed (0001) surface of ruthenium. This bilayer structure was initially adopted in first principle calculations of various metal surfaces [2, 14, 15, 16]. However, as more results on interfacial water structures became available, both experimentally and theoretically, the idea of an ice-like water bilayer was gradually abandoned [8, 11, 17, 18]. Low-energy electron diffraction (LEED) measurements [11] and density functional theory (DFT) calculations [17] have shown the relative instability of the bilayer water structure compared to a more stable water monolayer. More comprehensive discussion of models of water layers on metal surfaces can be found in the recent literature [19, 20, 21].

The dynamics of water layers on metal surfaces can be simulated with the *ab initio* molecular dynamics (AIMD) or classical molecular dynamics (CMD) techniques. While AIMD provides higher accuracy than CMD, it is computationally much more demanding and the resulting trajectories are usually too short to ensure sufficient statistical sampling of interface configurations [22, 23]. CMD simulations allow simulating longer times and larger systems, although often at the expense of accuracy [24]. The classical force fields-based approach has been also applied in some advanced hybrid DFT-classical molecular mechanics schemes

applied to metal-electrolyte interfaces, including the DFT/ESM-RISM (Effective Screening Medium-Reference Interaction Site Model) method [25, 26]. Simple force field-type approaches, or even the classical mean-field-type treatment, correctly capture some key interfacial properties like surface charging, alignment effects, dipole fields and variation in the dielectric constant of water at the interface, to name but a few [26, 27]. The accuracy of CMD and other force field-based approaches depends sensitively on the force field applied to describe interactions between molecules and atoms in the modeled system.

The interface force field (IFF) developed by Heinz et al. [28] is specifically designed to simulate solid-solvent interfaces; it includes interactions between certain metals and interfacial water molecules. However, studies of Berg et al. [9] and Steinmann et al. [29] revealed deficiencies of the IFF due to, for instance, neglecting Au-H and Pt-H interactions. It is thus worth further testing and improving the IFF parametrization for two reasons: (1) the IFF has not yet been widely tested for metal-water interfaces; (2) CMD is much more computationally efficient than AIMD and allows for simulation of larger systems and longer trajectories, and thus enables improved statistical sampling.

Here we focus on the investigation of the lead-water interface, an electrocatalytic system for CO_2 reduction [30, 31, 32, 33, 2, 34, 35, 36, 37], with formate as a product that is of significant value for various industrial uses, e.g. as a fuel in direct fuel cells or for the synthesis of pharmaceutical and crop protection products, to name but a few [38, 39, 40]. CMD results are compared to a previous AIMD study of water structures on lead [41]. Performing these studies serves two goals: (1) testing whether IFF-based CMD simulations could reproduce results of AIMD simulations and (2) testing the importance of time- and length-scales beyond those permitted by AIMD for the sampling of thermalized water structures at interfaces.

2. Computational details

2.1. Classical Molecular Dynamics (CMD) Computations

CMD simulations were performed with the LAMMPS software package [42]. The interatomic interactions were described by the interface force field (IFF) developed by Heinz et al. [28] and the SPC water model [43]. The interaction cutoff distance was set to 12 Å. Initial configurations of water on 2x2, 4x4, 6x6 and 8x8 Pb(100) surface unit cells were obtained by either DFT geometry optimization calculations (previously published or computed here) or random placement of water molecules, using the PACKMOL package [44]. More details on the configuration of water on the Pb surface will be given in the next section. MD simulations of a single water layer were performed at a temperature of 140 K under NVT conditions, using a timestep of 1 fs and a Nose-Hoover thermostat with temperature dumping parameter of 100 fs. This temperature was selected because it represents the desorption temperature of a single water layer [14] and was applied in the reference AIMD simulations [41]. For multiple water layers we performed CMD simulations at ambient temperature (300 K). In order to fully equilibrate the simulated systems, we produced 1000 ps long trajectories.

2.2. Density Functional Theory (DFT) Computations

Periodic DFT calculations of the 2x2 Pb(100) surface were performed using the Quantum-ESPRESSO package [45]. In order to allow direct comparison of our results with the DFT-AIMD study of Lin et al. [41], which we call here reference data (RD), we initially applied very similar computational setup with the PBE exchange correlation functional [46] and the plane wave cut-off energy of 50 Ry. We notice that our value is larger than the value of 30 Ry that had been used by Lin et al. [41], but we found that the higher value is required to assure proper

convergence of the electronic ground state energy. This difference may be a reason for some disagreements between our results and those of Lin et al. [41], which we discuss in Section 3.1. The projector augmented wave (PAW) method was used to describe the core electrons [47]. The 2x2 Pb(100) surfaces represented by a five-layers slab were created using the atomic simulation environment (ASE) [48]. To preserve the bulk-like environment, the two bottom Pb layers were kept fixed during the geometry optimization, while the other three layers were allowed to relax. A 20 Å vacuum space was created between the periodically repeated slabs to avoid any undesired interactions between them. A Monkhorst–Pack [49] 4x4x1 k-point grid was used. The calculated bulk Pb lattice constant of 5.03 Å is comparable to the measured value of 4.95 Å [34], and the observed overestimation of the lattice parameter is a usual feature of the PBE exchange-correlation functional [50].

3. Results and discussion

3.1. DFT calculations

We constructed the initial structures for CMD simulations using standard DFT calculations. For this purpose we performed DFT calculations with gradually increasing number of H_2O molecules added on the Pb(100) 2x2 surface unit cell. The adsorption energy per water molecule, E_{ads}, was calculated for each configuration as:

$$E_{ads} = (E_{tot} - E_{surf} - n * E_{water,iso})/n, \tag{1}$$

where E_{tot}, E_{surf} and $E_{water,iso}$ are the energies of the Pb-water system, the bare Pb(100) surface, and an isolated water molecule; n is the number of water molecules. A negative value of E_{ads} indicates stable surface adsorption.

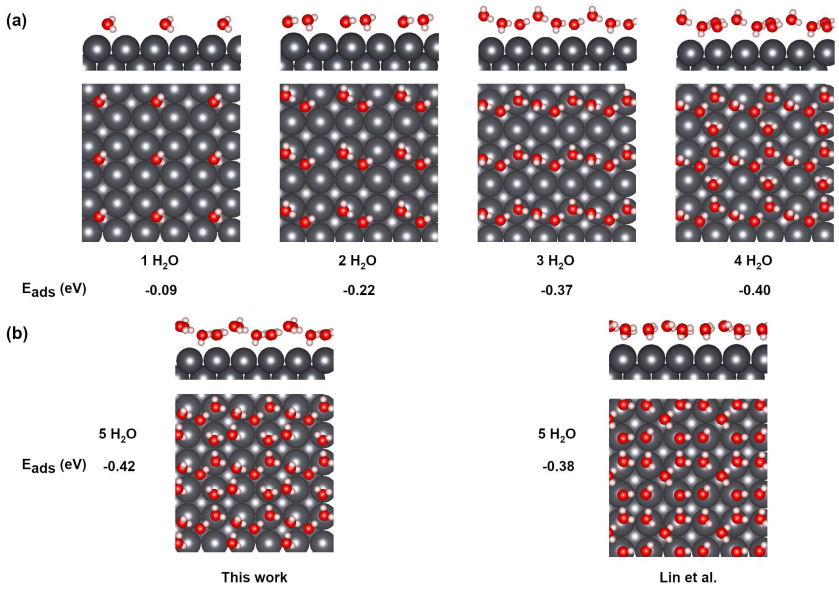

Figure 1: Top and side views of the computed water structures on Pb(100) surface ranging from a water coverage (in number of H_2O per unit surface) of (a) 1.25 to 1.00 and (b) 1.25. For comparative reasons, we also displayed the RD water structure of Lin et al. [41]. The corresponding DFT adsorption energies per water molecule are also provided. The relevant adsorption energies computed with the IFF are compared to the reported DFT values in Table S9. Red, white and grey colors mark oxygen, hydrogen and lead atoms, respectively.

The results for the most stable configuration with up to five surface water molecules are presented in Figure 1. A single water molecule adsorbs preferentially on the surface hollow site with one of its hydrogen atoms orientated toward the four-fold hollow site. The computed adsorption energy of a single water molecule is -0.09 eV, which indicates a very weak water-surface interaction. This is consistent with the weakly hydrophilic character of the Pb surface [51].

For $n = 2$, one of the water molecules is located near the top Pb site, while the second water molecule is located at the four-fold hollow site. The adsorption

energy per water molecule is -0.22 eV, because of the stabilizing hydrogen bonding between the two water molecules. Up until this point, both water structures and adsorption energies are in good agreement with the RD study. However, when adding the third adsorbed water molecule on the Pb(100) surface, a different configuration is found. Instead of the RD isolated triangular structure, we obtained a stripe-like structure. The average distance between water molecules remains at 2.74 Å, which is slightly smaller than in the water dimer configuration and in good agreement with the RD. E_{ads} is -0.37 eV, while Lin et al. [41] obtained a weaker adsorption energy of -0.27 eV. For a water coverage of four water molecules, we obtained a water structure that shows a decamer network (E_{ads}=-0.40 eV), while RD show a stripe-like structure (E_{ads}=-0.36 eV).

For a configuration with 5 water molecules we looked more closely at the difference between our water structure and that of RD, as this configuration is later used as the initial configuration for the classical MD simulations. While RD show a water network consisting of rectangles and distorted hexagons, our water structure consists of a mixture of pentamers and nonamers. We replicated the RD structure (see Figure S1 in the Supporting Information) and compared it to our most stable structure. In addition to the different water network, the adsorption energy of our structure is $E_{ads} = -0.42\,\mathrm{eV}$, while our calculations of the RD structure gave a slightly smaller adsorption energy of $-0.38\,\mathrm{eV}$. The difference in E_{ads} can be explained by the larger number of hydrogen bonds in our water network (6 hydrogen bonds per unit cell) than in the RD network consisting of rectangles and distorted hexagons (5 hydrogen bonds per unit cell). In the analysis we assumed formation of hydrogen bonding when the intermolecular O-H distance is smaller than 2.1 Å. The configurations with 6 or more water molecules could not be stabilized, with additional molecules being pushed up out of the surface water layer. The corresponding water adsorption energies computed with the IFF for all the cases

discussed above are provided in Table S9. These are very similar to the reported DFT values and both sets of results show identical trend with increasing number of water molecules.

To summarize our *ab initio* investigation, we have observed some differences from RD studies [41] for local stable water network configurations using unit cells with 3, 4 and 5 water molecules. This led us to two different initial configurations for classical MD simulations, which shows that it is not trivial to find a correct water structure with the applied *"by hand"* method. In that respect, MD simulations could be valuable for finding an equilibrium water structure. We thus selected the two obtained structures at $n = 5$ (ours and RD) as the initial structure for CMD simulations of a full water monolayer on the Pb(100) surface.

3.2. Classical Molecular Dynamics (CMD) simulations of single water layer

To evaluate the feasibility of IFF-based CMD for the investigation of water structures on the Pb(100) surface, we selected the two water structures with $n = 5$, computed with DFT as the initial configurations (ours and RD, see Section 3.1). As CMD allows for much longer simulation times than AIMD, we ran simulations for 1000 ps (compared to 8 ps AIMD runs [41]). We will show that such a long simulation time is necessary to ensure well equilibrated surface water structures.

The CMD simulation results are presented in Figures 2 and S3. Using the RD water structure as the initial configuration, we obtained a good agreement between CMD simulations and the AIMD data. At 8 ps, AIMD and CMD simulations show a water network consisting of rectangles and distorted hexagons (Figure 2 (a)). This water network comprises of one H-up water (one hydrogen of the water molecule pointing away from the surface) and one H-down water (one hydrogen of the water molecule pointing towards the surface). However, detailed analysis of the structural evolution along the MD trajectory, as represented by Figure S3(a) (and related Fig-

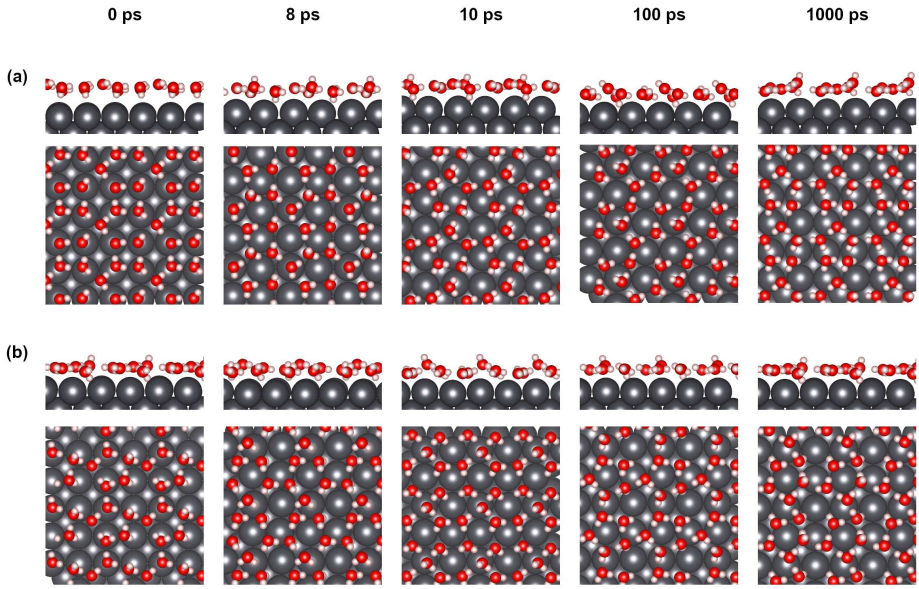

Figure 2: Snapshots of CMD simulations of single water layer on Pb(100) surface using (a) RD structure [41] and (b) our DFT structure as initial conditions, in side and top views at different time steps. The water coverage is 1.25/unit surface. Red, white and grey colors represent oxygen, hydrogen and lead atoms, respectively.

ures S3 (b)-(d) obtained from simulations with larger surface cells) clearly shows that 8 ps is too short to ensurre equilibration; the equilibrium is reached only after a few hundred picoseconds. Thus, the water network that consists of rectangles and distorted hexagons transformed substantially after short simulation time. At 10 ps, a network consisting of pentamers and nonamers formed, agreeing well with our DFT-based initial configuration (Figure 2 (b)). While the water network of pentamers and nonamers transforms into a more disordered structure at 100 ps, it is restored at 1000 ps. The time evolution (Figure S3(a)) shows that this structure is dominant, with an occurrence level at $\sim$ 50% (Table 1). Based on the trajectory analysis, at 1000 ps the system has reached thermal equilibrium (Figure S2.1 and

S3(a) in the Supporting Information). Thus, based on these findings we conclude the following: (1) CMD simulations are capable of recreating the same water structure as the AIMD simulations at the same simulation time scale, (2) a few ps long AIMD simulations are not sufficient to attain equilibrated water structures and (3) our DFT-based water structure closely resembles the final structure obtained with CMD at 1000 ps.

In order to test further the thermal stability of the proposed structure, we ran the CMD simulations taking our DFT-based structure as the initial configuration. Figure 2 (b) shows snapshots of classical MD simulations for this case. After 1000 ps the initial structure was preserved, indicating its stability. Interestingly, at 10 ps we observe a transition from the mixed pentamer and nonamer water structure to a rectangular and distorted hexagonal water network (i.e., the RD structure). This indicates that the RD water network is an intermediate or a metastable state. The analysis of the structural evolution along the entire CMD trajectory indicates that such a structure occures with a probability of only 8% (Table 1). This is a consequence of the energy difference between the two structures (0.04 eV (DFT), 0.03 eV (IFF), Table S10), as already discussed in the previous section.

We also ran CMD simulations using a random initial water configuration generated with the aid of PACKMOL package (see Figure S4 in the Supporting information). Even starting with a random initial water configuration, after 1000 ps we obtained a mixed pentamer and nonamer water structure. This observation strengthens our finding that the mixed pentamer and nonamer network is the most stable water structure in the equilibrium state at the 2x2 surface unit cell.

To further quantify the differences in the obtained water structures, we analyzed the distance of the water layer to the Pb(100) surface as presented in Table 2. The first row in Table 2 (”DFT”) represents the stable water structure obtained in our DFT calculation. (Figure 2 (b) at 0 ps). The first oxygen atom is located

Table 1: Statistical occurrence of different water network polygons at the Pb(100) surface simulated with single water layer and different surface unit cells. Analysis was performed on equilibrated parts of trajectory (from 500ps to 1000ps). The most frequently occuring polygons are marked in bold. The errors are computed as standard error of the mean (confidence level of 68%).

Surface size	**Relative occurrence of polygons [%]**						
	Triangle	Rectangle	Pentagon	Hexagon	Heptagon	Octagon	Nonagon
2x2	4.8 ± 1.9	8.0 ± 2.5	**39.5 ± 4.0**	4.0 ± 2.3	0.0 ± 0.0	8.0 ± 2.8	**35.7 ± 4.4**
4x4	5.5 ± 0.6	**28.5 ± 1.4**	**33.8 ± 1.1**	19.0 ± 1.4	11.2 ± 1.4	1.5 ± 0.5	0.5 ± 0.3
6x6	3.6 ± 0.4	**41.2 ± 0.8**	**32.1 ± 0.9**	11.3 ± 0.6	6.0 ± 0.5	5.2 ± 0.5	0.6 ± 0.2
8x8	2.4 ± 0.2	**52.3 ± 0.8**	**26.3** ± 0.7	10.2 ± 0.5	5.5 ± 0.4	2.0 ± 0.2	1.3 ± 0.2

at 3.34 Å above the Pb surface, while the maximum Pb-O distance is at 4.51 Å. Optimization with the IFF, initialized with that structure, places the water layer in closer proximity to the surface, with the Pb-O distance ranging from 2.55 Å to 3.38 Å.

Table 2: Comparison of first layer water molecules-Pb(100) surface distance simulated with the 2x2 surface unit cell using different computational methods. The first two rows show results for water configurations obtained with DFT and DFT+D3 (dispersive corrections). The last row shows the result for the water structure arrived at via IFF optimization that started from an initial geometry optimized by DFT.

Computational method	**Range of Pb-O distance [Å]**	**Average Pb-O distance [Å]**
DFT	3.34 - 4.51	3.81
DFT + D3	3.20 - 4.21	3.63
IFF (DFT)	2.55 - 3.38	3.09

From our analysis of the water-metal distance we conclude that, even though we are able to find identical water structures in MD and DFT calculations (mixed pentamers and nonamers water structure), the Pb-O distances found with the IFF

differ significantly from those found with DFT. It is known that adding dispersion correction to DFT may be crucial to assure the stability of water structures on metal surfaces [52]. However, adding dispersion corrections in our case (”DFT + D3”) does not change the structure of the water network (Figure S5 in the Supporting Information). However, it shifts the Pb-O distances slightly to lower values (Table 2), yet not enough to reconcile CMD and DFT Pb-O distances. The main reason for the deviation between our IFF-based and DFT simulations is an inadequate or incomplete description of water-surface interactions. Berg et al. [9] and Steinmann et al. [29] discussed the difficulty of the IFF to correctly capture the Pb-H interactions. Polarization effects, which are crucial for the correct description of metal surface-adsorbate interactions [53], are not accounted for in the IFF applied here. Nevertheless, the water structure is determined mainly by the applied water model and the distribution of surface Pb atoms is determined by the lattice parameter, to which water layer tries to accommodate. It should not be affected by the strength of direct interactions between surface atoms and water molecules, which determines mainly the distance of the water layer from the surface.

3.2.1. Surface size effect

Another aspect that we test here is the effect of size of surface cell model on the water structures at the Pb(100) surface. For larger surface cells, we have to resort to CMD simulations since the AIMD approach becomes prohibitively expensive. Figure 3 shows geometry snapshots at different CMD timeframes for 4x4, 6x6 and 8x8 surface unit cells, using as the initial water structure the configuration obtained with the 2x2 surface unit cell model (Figure 2 (b) at 0 ps). For all three surface sizes, we observe a quick destabilization of the mixed pentamer and nonamer water structure. Interestingly, no ordered structure is obtained after 1000 ps in all the cases. Instead, a large cavity is formed. The cavity can be easily filled out with

Table 3: Statistical occurrence of different water network polygons at Pb(100) surface simulated with thick water slab at different surface unit cells. Analysis was performed on equilibrated parts of trajectory (from 500ps to 1000ps). The most frequently occuring polygons are marked in bold. The errors are computed as standard error of the mean (confidence level of 68%).

Surface size	**Relative occurrence of polygons [%]**						
	Triangle	Rectangle	Pentagon	Hexagon	Heptagon	Octagon	Nonagon
2x2	8.5 ± 3.5	5.9 ± 2.6	**46.7 ± 6.8**	0.0 ± 0.0	0.0 ± 0.0	1.7 ± 1.8	**37.2 ± 6.8**
4x4	9.4 ± 1.0	**16.9 ± 1.2**	**24.7 ± 1.7**	**21.2 ± 1.5**	12.0 ± 1.2	6.6 ± 1.0	9.2 ± 1.2
6x6	9.5 ± 0.6	**17.3 ± 0.8**	**27.5 ± 1.2**	**20.7 ± 1.0**	11.0 ± 0.8	6.8 ± 0.5	7.2 ± 0.7
8x8	8.1 ± 0.4	**17.1 ± 0.6**	**25.7 ± 0.7**	**19.3 ± 0.7**	11.5 ± 0.6	9.6 ± 0.5	8.7 ± 0.6

additional water molecules, which indicates more denser water layer than the one obtained when simulating the 2x2 surface.

To derive such a structure we filled up the water cavity with additional water molecules until a full monolayer of H_2O is formed. The procedure we applied to fill up the water cavity is described in more details in Figure S6 in the Supporting Information. After filling up the first water layer, we ran CMD simulations to equilibrate the structures. Figure 4 shows the variation of the water density along the normal to the Pb surface for the computed surface unit cells. It is evident that in case of the 2x2 surface unit cell the first density peak (at 3 Å) is sharper and shifted slightly to the left, as compared to the broader peaks obtained for larger simulated surface cells. The sharper peak indicates overstructuring of the water layer. It is clear that for a realistic description of water structures, at least a 4x4 surface unit cell should be used. Table 4 compares the number of H_2O molecules in the first layer for each surface configuration. We found that the 4x4, 6x6 and 8x8 structures incorporate ~ 1.5 H_2O molecules/unit surface area, while the 2x2 surface unit cell

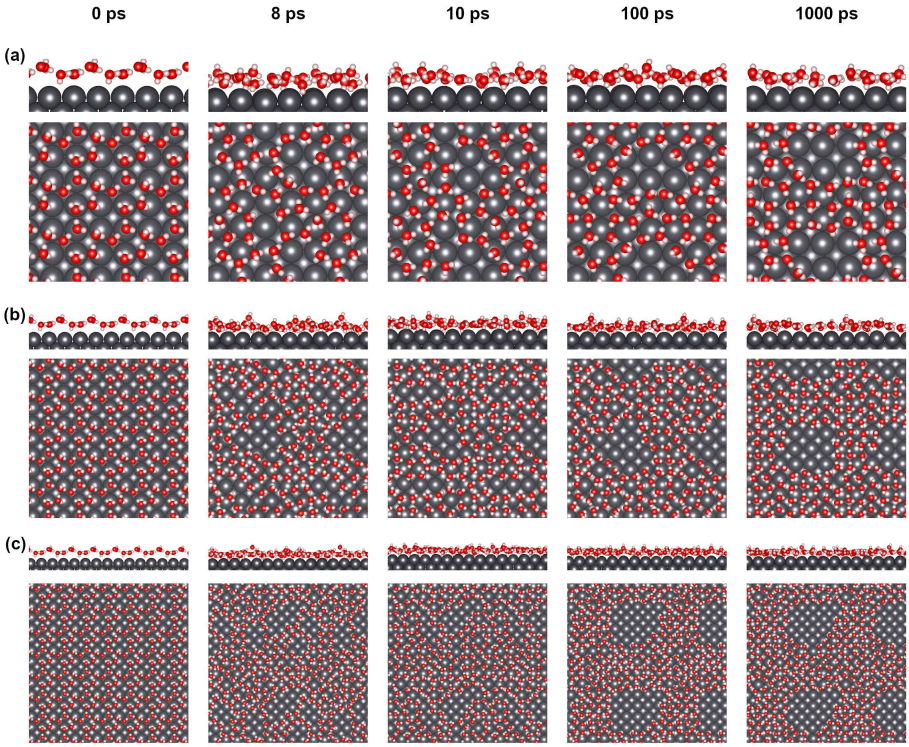

Figure 3: Snapshots of CMD simulations of single water layer simulated with the (a) 4x4, (b) 6x6 and (c) 8x8 Pb(100) surface unit cells, in side and top views at different time steps. The water coverage for all configurations is 1.25/unit surface. Red, white and grey colors represent oxygen, hydrogen and lead atoms, respectively.

allows for only 1.25 H_2O molecules/unit surface area. This shows a clear limitation of using the small 2x2 surface unit cells for investigation of water structure on metal surfaces. Figures S3 (a)-(d) show the structural evolution of the surface water layer. The frequency of appearances of different structural configurations are given in Table 1. It is clear that rectangle-pentagon configurations prevail in all cases. It is also evident that, as in the case of 2x2 cell, equilibration is very slow and takes a few hundred picoseconds. Such a long simulation times are currently

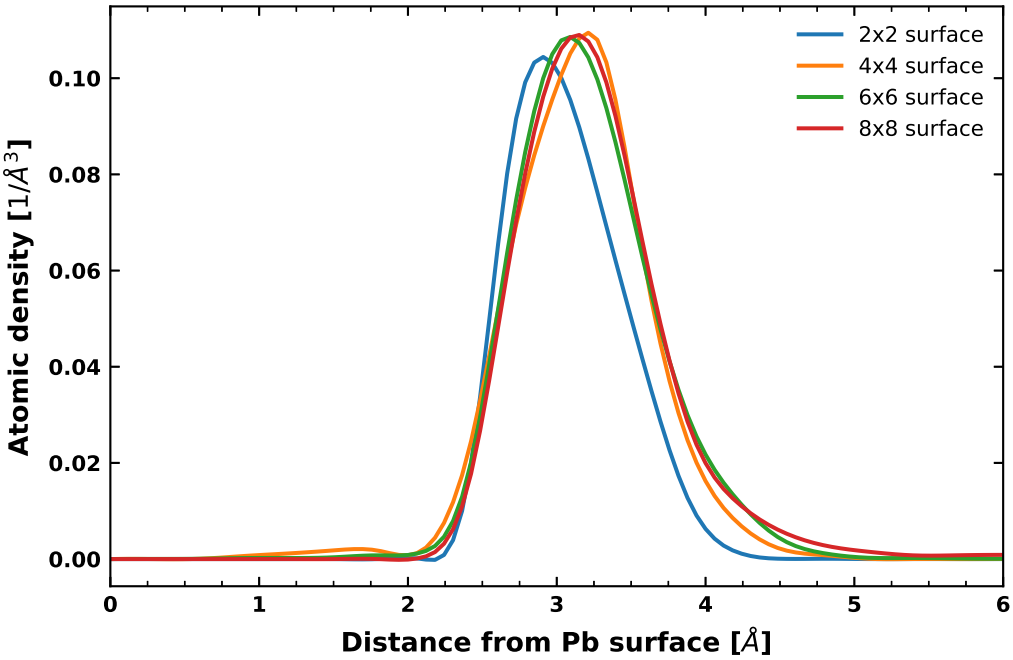

Figure 4: Water density distribution of first layer H_2O molecules on Pb(100) surface obtained with 2x2, 4x4, 6x6 and 8x8 surface unit cells. The results from simulations of single water layer.

prohibitive for any AIMD simulations on a reasonable computational resources.

3.3. CMD simulations of thick water slab

In order to obtain the most realistic water structure we filled up the entire vacuum layer with H_2O molecules and ran the MD simulations at a temperature of 300K. We fixed the water density to 1 g/L for all simulations. Figure 5 shows the obtained atomic density profile for oxygen along the normal to the Pb surface. As in simulations with a single water layer, we observe a slight deviation of the water density profile obtained with the 2x2 surface unit cell. While there is

Table 4: Number of H_2O molecules (per surface unit cell) in the surface water layer at Pb(100) for different surface unit cells. A single water layer was considered.

Surface size	**No. of H_2O molecules**
2x2	1.25
4x4	1.56
6x6	1.56
8x8	1.53

a good agreement in the height and location of first peak (at $\sim$ 3 Å), the second peak is slightly higher. In addition, the remaining peaks are on average much more ”dispersed” than the density profiles obtained with larger surface unit cells show. This strengthens the argument that the 2x2 surface is too confined for simulations of ”realistic” water structures. Nevertheless, the water density profiles are in good agreement with the density profiles at water-metal interfaces found in other simulations [53, 54, 9]. Table 5 shows the obtained density of first layer water molecules. For all surface cell sizes the number of first layer water molecules is very similar ($\sim$ 1.5 Å), and consistent with that obtained from the single layer studies with large surface cells (Table 4). Results of the statistical analysis of structural evolution of the surface water layer are provided in Table 3. It qualitatively resembles the one obtained with a single water layer and shows the appearance of rectangle-pentagon structure. This validates the computational approaches that employs a surface water layer to simulate the effect of surface hydration [20, 21].

3.4. CMD simulations of water structure on Pb(111)

We have conducted CMD simulations with a single layer of H_2O and the cell filled completely with H_2O of 1g/L density for the Pb(111) surface. In these, we

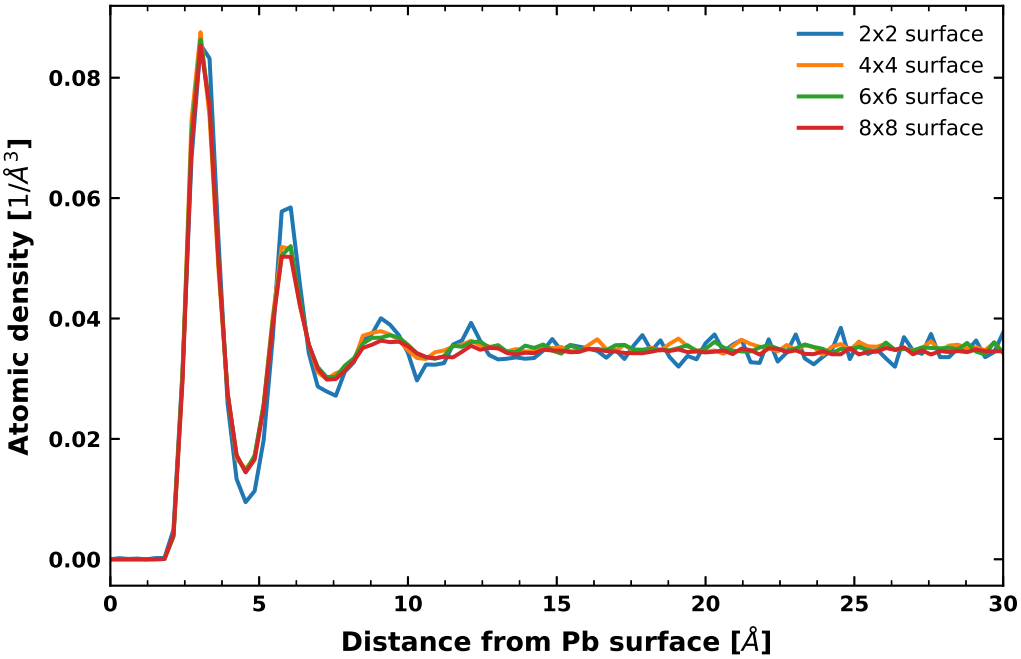

Figure 5: Water density distribution obtained with different surface unit cells for the Pb(100) surface. The results from simulations with thick water slab.

Table 5: Comparison of number of first layer H_2O molecules at Pb(100) surfaces obtained from simulations of different surface unit cell sizes. The results from simulations with thick water slab.

Surface size	**No. of H_2O molecules**
2x2	1.52
4x4	1.48
6x6	1.48
8x8	1.45

observe a higher instability of the water layer on the Pb(111) surface compared to the Pb(100) surface (Figure S2.2 in the Supporting Information). Comparison of the equilibrated water layer structures at Pb(111) and Pb(100) surfaces reveals the formation of a water bilayer on the Pb(111) surface, which was not seen at Pb(100). This agrees with the RD [41]. As illustrated in Figure 6, in the case of the inter-slab space completely filled with water, the density profile of water on the Pb(111) surface shows some differences in the height of the first two peaks compared to the Pb(100) surface. The first peaks are much more pronounced in the case of the Pb(111) surface, indicating the greater distance between first two water layers. This was also observed in the RD AIMD simulations [41]. Furthermore, the interfacial density of H_2O varies between both Pb surfaces, with the Pb(100) and Pb(111) surfaces having the surface water layer density of 1.50 and 1.25 per unit surface, respectively. In general, the Pb(111) surface exhibits a weaker Pb-water interaction than the Pb(100) surface, which is consistent with AIMD RD [41].

4. Conclusions

With the IFF-based CMD simulations we have performed a comprehensive investigation of water structures on the Pb(100) and (111) surfaces and found water

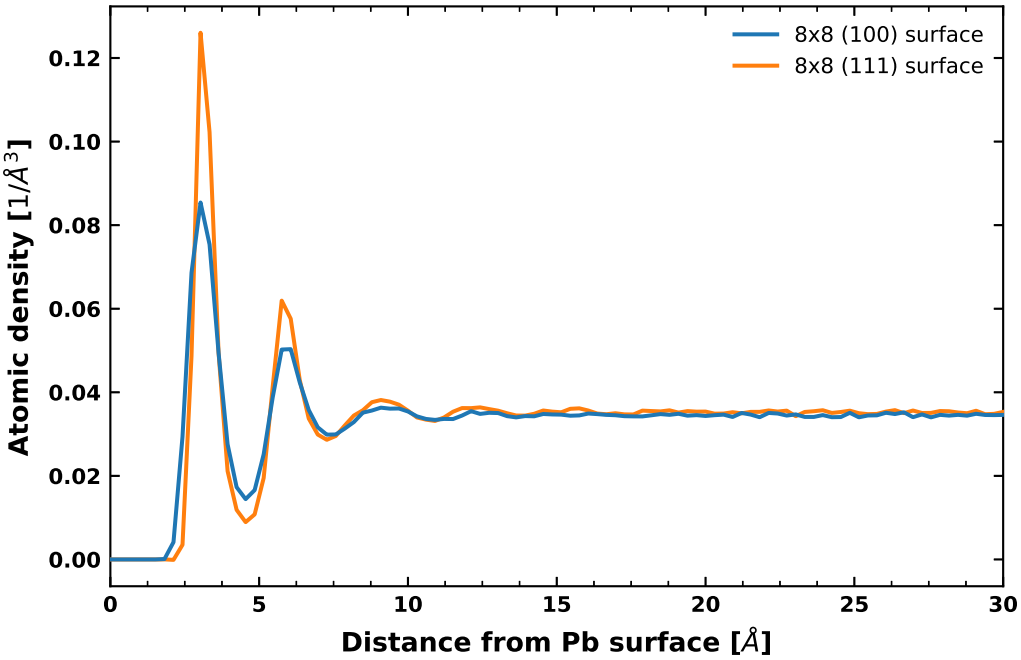

Figure 6: Water density distribution obtained with 8x8 surface unit cell for the Pb(100) and Pb(111) surfaces. The results from simulations with thick water slab.

structures that are consistent with those obtained with AIMD simulations, when applying similar simulation time and length constrains. However, we found that the limited simulation time (up to a few ps) and small surface unit cells permitted by the AIMD simulations cannot guarantee obtaining equilibrated water structures. We obtained well-equilibrated water structures with much longer CMD simulations (ns and longer vs. ps) and noticed that at least 4x4 surface unit cells must be used to produce realistic water structures. We observed that the water-equilibrated Pb(100) and (111) surfaces have 1.50 and 1.25 water molecules per unit surface, respectively. On the other hand, although the IFF can correctly capture the water

structure, the water-surface distance is significantly underestimated due to an incomplete description of metal-adsorbate interactions. Nevertheless, the fact that the surface water structure can be correctly reproduced by IFF is an important result, given the superior computational efficiency of CMD as compared to the AIMD approach, a crucial factor for realistic equilibration and statistical sampling.

Acknowledgements

We acknowledge the computational resources on RWTH Aachen University and Forschungszentrum Jülich provided by JARA-CSD.

References

[1] J. K. Nørskov, T. Bligaard, J. Rossmeisl, C. H. Christensen, Towards the computational design of solid catalysts, Nat. Chem. 1 (1) (2009) 37–46.

[2] C. X. Zhao, Y. F. Bu, W. Gao, Q. Jiang, CO_2 Reduction Mechanism on the Pb(111) Surface: Effect of Solvent and Cations, J. Phys. Chem. C 121 (36) (2017) 19767–19773.

[3] Z. Tian, C. Priest, L. Chen, Recent Progress in the Theoretical Investigation of Electrocatalytic Reduction of CO_2, Adv. Theory Simul. 1 (5) (2018) 1800004.

[4] O. M. Magnussen, A. Groß, Toward an Atomic-Scale Understanding of Electrochemical Interface Structure and Dynamics, J. Am. Chem. Soc. 141 (12) (2019) 4777–4790.

[5] I. Ledezma-Yanez, W. D. Z. Wallace, P. Sebastián-Pascual, V. Climent, J. M. Feliu, M. T. M. Koper, Interfacial water reorganization as a pH-dependent

descriptor of the hydrogen evolution rate on platinum electrodes 2 (4) (2017) 17031.

[6] A. Michaelides, Density functional theory simulations of water–metal interfaces: waltzing waters, a novel 2D ice phase, and more, Appl. Phys. A 85 (4) (2006) 415–425.

[7] S. Sakong, A. Groß, Water structures on a Pt(111) electrode from *ab initio* molecular dynamic simulations for a variety of electrochemical conditions, Phys. Chem. Chem. Phys. 22 (19) (2020) 10431–10437.

[8] A. Groß, F. Gossenberger, X. Lin, M. Naderian, S. Sakong, T. Roman, Water Structures at Metal Electrodes Studied by Ab Initio Molecular Dynamics Simulations, J. Electrochem. Soc. 161 (8) (2014) E3015–E3020.

[9] A. Berg, C. Peter, K. Johnston, Evaluation and Optimization of Interface Force Fields for Water on Gold Surfaces, J. Chem. Theory Comput. 13 (11) (2017) 5610–5623.

[10] M. Tatarkhanov, D. F. Ogletree, F. Rose, T. Mitsui, E. Fomin, S. Maier, M. Rose, J. I. Cerdá, M. Salmeron, Metal- and Hydrogen-Bonding Competition during Water Adsorption on Pd(111) and Ru(0001), J. Am. Chem. Soc. 131 (51) (2009) 18425–18434.

[11] G. Held, D. Menzel, Isotope effects in structure and kinetics of water adsorbates on Ru(001), Surf. Sci. 327 (3) (1995) 301–320.

[12] F. McBride, A. Omer, C. M. Clay, L. Cummings, G. R. Darling, A. Hodgson, Strain relief and disorder in commensurate water layers formed on Pd(111), J. Phys.: Condens. Matter 24 (12) (2012) 124102.

[13] D. L. Doering, T. E. Madey, The adsorption of water on clean and oxygen-dosed Ru(011), Surf. Sci. 123 (2) (1982) 305 – 337.

[14] X. Lin, A. Groß, First-principles study of the water structure on flat and stepped gold surfaces, Surf. Sci. 606 (11) (2012) 886–891.

[15] S. Schnur, A. Groß, Properties of metal–water interfaces studied from first principles, New J. Phys. 11 (12) (2009) 125003.

[16] Y. Gohda, S. Schnur, A. Groß, Influence of water on elementary reaction steps in electrocatalysis, Faraday Discuss. 140 (2009) 233–244.

[17] P. J. Feibelman, Partial Dissociation of Water on Ru(0001), Science 295 (5552) (2002) 99–102.

[18] M. Naderian, A. Groß, From single molecules to water networks: Dynamics of water adsorption on Pt(111), J. Chem. Phys. (2016) 8.

[19] A. Groß, Theory of Solid/Electrolyte Interfaces, Surface and Interface Science, WILEY-VCH Verlag GmbH & Co., 471–515, 2020.

[20] O. Björneholm, M. H. Hansen, A. Hodgson, L.-M. Liu, D. T. Limmer, A. Michaelides, P. Pedevilla, J. Rossmeisl, H. Shen, G. Tocci, E. Tyrode, M.-M. Walz, J. Werner, H. Bluhm, Water at Interfaces, Chem. Rev. 116 (13) (2016) 7698–7726.

[21] J. Carrasco, A. Hodgson, A. Michaelides, A molecular perspective of water at metal interfaces, Nat. Mater. 11 (8) (2012) 667–674.

[22] G. Cicero, A. Calzolari, S. Corni, A. Catellani, Anomalous Wetting Layer at the Au(111) Surface, J. Phys. Chem. Lett. 2 (20) (2011) 2582–2586.

[23] T. Ludwig, J. A. Gauthier, K. S. Brown, S. Ringe, J. K. Nørskov, K. Chan, Solvent–Adsorbate Interactions and Adsorbate-Specific Solvent Structure in Carbon Dioxide Reduction on a Stepped Cu Surface, J. Phys. Chem. C 123 (10) (2019) 5999–6009.

[24] C. Peter, K. Kremer, Multiscale simulation of soft matter systems – from the atomistic to the coarse-grained level and back, Soft Matter 5 (22) (2009) 4357.

[25] S. Nishihara, M. Otani, Hybrid solvation models for bulk, interface, and membrane: Reference interaction site methods coupled with density functional theory, Phys. Rev. B 96 (2017) 115429.

[26] R. Tesch, P. M. Kowalski, M. H. Eikerling, Properties of the Pt(111)/electrolyte electrochemical interface studied with a hybrid DFT–solvation approach, J. Phys.: Condens. Matter 33 (44) (2021) 444004.

[27] J. Huang, S. Chen, M. Eikerling, Grand-Canonical Model of Electrochemical Double Layers from a Hybrid Density–Potential Functional, J. Chem. Theory Comput. 17 (4) (2021) 2417–2430.

[28] H. Heinz, T.-J. Lin, R. Kishore Mishra, F. S. Emami, Thermodynamically Consistent Force Fields for the Assembly of Inorganic, Organic, and Biological Nanostructures: The INTERFACE Force Field, Langmuir 29 (6) (2013) 1754–1765.

[29] S. N. Steinmann, R. Ferreira De Morais, A. W. Götz, P. Fleurat-Lessard, M. Iannuzzi, P. Sautet, C. Michel, Force Field for Water over Pt(111): De-

velopment, Assessment, and Comparison, J. Chem. Theory Comput. 14 (6) (2018) 3238–3251.

[30] Y. Hori, Electrochemical CO2 Reduction on Metal Electrodes, in: C. G. Vayenas, R. E. White, M. E. Gamboa-Aldeco (Eds.), Modern Aspects of Electrochemistry, vol. 42, Springer New York, 89–189, 2008.

[31] J. S. Yoo, R. Christensen, T. Vegge, J. K. Nørskov, F. Studt, Theoretical Insight into the Trends that Guide the Electrochemical Reduction of Carbon Dioxide to Formic Acid, ChemSusChem 9 (4) (2016) 358–363.

[32] Z. Yang, F. E. Oropeza, K. H. L. Zhang, P-block metal-based (Sn, In, Bi, Pb) electrocatalysts for selective reduction of CO_2 to formate, APL Materials 8 (6) (2020) 060901.

[33] S. Nitopi, E. Bertheussen, S. B. Scott, X. Liu, A. K. Engstfeld, S. Horch, B. Seger, I. E. L. Stephens, K. Chan, C. Hahn, J. K. Nørskov, T. F. Jaramillo, I. Chorkendorff, Progress and Perspectives of Electrochemical CO_2 Reduction on Copper in Aqueous Electrolyte, Chem. Rev. 119 (12) (2019) 7610–7672.

[34] M. Fan, M. J. Eslamibidgoli, S. Garbarino, A. C. Tavares, M. H. Eikerling, D. Guay, A Computational-Experimental Investigation of the Mechanisms Responsible for the Enhanced CO2 Electrochemical Reduction of Dendritic Sn1Pb3 Alloy, J. Electrochem. Soc. MA2020-01 (24) (2020) 17953–17979.

[35] C. H. Lee, M. W. Kanan, Controlling H^+ vs CO_2 Reduction Selectivity on Pb Electrodes, ACS Catal. 5 (1) (2015) 465–469.

[36] S. Y. Choi, S. K. Jeong, H. J. Kim, I.-H. Baek, K. T. Park, Electrochemical

Reduction of Carbon Dioxide to Formate on Tin–Lead Alloys, ACS Sustainable Chem. Eng. 4 (3) (2016) 1311–1318.

[37] C. Cui, H. Wang, X. Zhu, J. Han, Q. Ge, A DFT study of CO2 electrochemical reduction on Pb(211) and Sn(112), Sci. China Chem. 58 (4) (2015) 607–613.

[38] A. K. Singh, S. Singh, A. Kumar, Hydrogen energy future with formic acid: a renewable chemical hydrogen storage system, Catal. Sci. Technol. 6 (1) (2016) 12–40.

[39] J. Klankermayer, S. Wesselbaum, K. Beydoun, W. Leitner, Selective Catalytic Synthesis Using the Combination of Carbon Dioxide and Hydrogen: Catalytic Chess at the Interface of Energy and Chemistry, Angew. Chem. Int. Ed. 55 (26) (2016) 7296–7343.

[40] J. Hietala, A. Vuori, P. Johnsson, I. Pollari, W. Reutemann, H. Kieczka, Formic Acid, in: Wiley-VCH Verlag GmbH & Co. KGaA (Ed.), Ullmann's Encyclopedia of Industrial Chemistry, Wiley-VCH Verlag GmbH & Co. KGaA, 1–22, 2016.

[41] X. Lin, F. Evers, A. Groß, First-principles study of the structure of water layers on flat and stepped Pb electrodes, Beilstein J. Nanotechnol. 7 (2016) 533–543.

[42] S. Plimpton, Fast Parallel Algorithms for Short-Range Molecular Dynamics, J. Comput. Phys. 117 (1) (1995) 1 – 19.

[43] H. J. C. Berendsen, J. R. Grigera, T. P. Straatsma, The missing term in effective pair potentials, J. Phys. Chem. 91 (24) (1987) 6269–6271.

[44] L. Martínez, R. Andrade, E. G. Birgin, J. M. Martínez, PACKMOL: A package for building initial configurations for molecular dynamics simulations, J. Comput. Chem. 30 (13) (2009) 2157–2164.

[45] P. Giannozzi, S. Baroni, N. Bonini, M. Calandra, R. Car, C. Cavazzoni, D. Ceresoli, G. L. Chiarotti, M. Cococcioni, I. Dabo, A. D. Corso, S. de Gironcoli, S. Fabris, G. Fratesi, R. Gebauer, U. Gerstmann, C. Gougoussis, A. Kokalj, M. Lazzeri, L. Martin-Samos, N. Marzari, F. Mauri, R. Mazzarello, S. Paolini, A. Pasquarello, L. Paulatto, C. Sbraccia, S. Scandolo, G. Sclauzero, A. P. Seitsonen, A. Smogunov, P. Umari, R. M. Wentzcovitch, QUANTUM ESPRESSO: a modular and open-source software project for quantum simulations of materials, J. Phys.: Condens. Matter 21 (39) (2009) 395502.

[46] J. P. Perdew, K. Burke, M. Ernzerhof, Generalized Gradient Approximation Made Simple, Phys. Rev. Lett. 77 (1996) 3865–3868.

[47] P. E. Blöchl, Projector augmented-wave method, Phys. Rev. B 50 (24) (1994) 17953–17979.

[48] A. Hjorth Larsen, J. Jørgen Mortensen, J. Blomqvist, I. E. Castelli, R. Christensen, M. Dułak, J. Friis, M. N. Groves, B. Hammer, C. Hargus, E. D. Hermes, P. C. Jennings, P. Bjerre Jensen, J. Kermode, J. R. Kitchin, E. Leonhard Kolsbjerg, J. Kubal, K. Kaasbjerg, S. Lysgaard, J. Bergmann Maronsson, T. Maxson, T. Olsen, L. Pastewka, A. Peterson, C. Rostgaard, J. Schiøtz, O. Schütt, M. Strange, K. S. Thygesen, T. Vegge, L. Vilhelmsen, M. Walter, Z. Zeng, K. W. Jacobsen, The atomic simulation environment—a Python library for working with atoms, J. Phys.: Condens. Matter 29 (27) (2017) 273002.

[49] H. J. Monkhorst, J. D. Pack, Special points for Brillouin-zone integrations, Phys. Rev. B 13 (12) (1976) 5188–5192.

[50] J. P. Perdew, A. Ruzsinszky, G. I. Csonka, O. A. Vydrov, G. E. Scuseria, L. A. Constantin, X. Zhou, K. Burke, Restoring the Density-Gradient Expansion for Exchange in Solids and Surfaces, Phys. Rev. Lett. 100 (2008) 136406.

[51] J. H. Park, N. R. Aluru, Diffusion of water submonolayers on hydrophilic surfaces, Applied Physics Letters 93 (25) (2008) 253104, doi: 10.1063/1.3054640.

[52] P. J. Feibelman, Using Ar adsorption to estimate the van der Waals contribution to the wetting of Ru(0001), Phys. Rev. B: Condens. Matter Mater. Phys. (2005) 3.

[53] I. L. Geada, H. Ramezani-Dakhel, T. Jamil, M. Sulpizi, H. Heinz, Insight into induced charges at metal surfaces and biointerfaces using a polarizable Lennard–Jones potential, Nat. Commun. (2018) 14.

[54] H. H. Heenen, J. A. Gauthier, H. H. Kristoffersen, T. Ludwig, K. Chan, Solvation at metal/water interfaces: An *ab initio* molecular dynamics benchmark of common computational approaches, J. Chem. Phys. 152 (14) (2020) 144703.